We are IntechOpen, the world's leading publisher of Open Access books
Built by scientists, for scientists

6,900
Open access books available

185,000
International authors and editors

200M
Downloads

154
Countries delivered to

Our authors are among the

TOP 1%
most cited scientists

12.2%
Contributors from top 500 universities

CLARIVATE ANALYTICS
BOOK CITATION INDEX
INDEXED

WEB OF SCIENCE™

Selection of our books indexed in the Book Citation Index
in Web of Science™ Core Collection (BKCI)

Interested in publishing with us?
Contact book.department@intechopen.com

Numbers displayed above are based on latest data collected.
For more information visit www.intechopen.com

LEPTS — a Radiation-Matter Interaction Model at the Molecular Level and its Use in Biomedical Applications

Martina Fuss[1], Ana G. Sanz[1], Antonio Muñoz[2],
Francisco Blanco[3], Marina Téllez[4], Carlos Huerga[4] and Gustavo García[1]
[1]*Instituto de Física Fundamental, Consejo Superior de Investigaciones Científicas*
[2]*Centro de Investigaciones Energéticas, Medioambientales y Tecnológicas (CIEMAT)*
[3]*Departamento de Física Atómica, Molecular y Nuclear,*
Universidad Complutense de Madrid
[4]*Hospital Universitario La Paz, Madrid*
Spain

1. Introduction

Monte Carlo-based simulations of radiation transport through biological tissues constitute an important complement to experimental dosimetry for the assessment of radiation damage in radioprotection as well as clinical applications such as diagnostics and radiotherapy. In comparison with conventional dose calculation methods that combine empirical data and deterministic algorithms, they offer significant improvements (Reynaert et al., 2007) particularly in conditions involving inhomogeneous materials or geometrically complex irradiation conditions. Therefore, various Monte Carlo (MC) codes oriented towards radiotherapeutic (Berger & Seltzer, 1973; Kawrakow, 2000; Brown, 2003; Baró et al., 1995; Agostinelli, 2003; Halbleib & Melhorn, 1984) and medical imaging (Jan, 2004; Badano & Sempau, 2006) applications have been developed in the last decades. Those programmes provide particle tracking making use of public reference databases such as Storm & Israel (1970); Cullen et al. (1997); Hubbell et al. (1975; 1985); Perkins et al. (1991b); ICRU (1984); Perkins et al. (1991a); Seltzer & Berger (1985) (for a summary, see table 1 in Verhaegen & Seuntjens (2003)) and include sophisticated elements that help reduce calculation time, e.g. condensed-history algorithms. Additionally, electrons are usually forced to instantly deposit all of their remaining energy below a certain cut-off value, further speeding up simulations. Generally, energy deposition in a given volume is assumed to be directly proportional to the number of ionization events that have been produced therein.

However, during the irradiation of biological tissues and almost irrespective of the incident radiation quality, a considerable portion of energy dose is eventually deposited in the target material by secondary electrons through multiple collisions. Only recent discoveries have shown that molecular damage (e.g., molecular dissociations or strand breaks in DNA) can be induced in biomolecules very efficiently even by sub-ionising electrons through molecular resonances (Boudaïffa et al., 2000; Huels et al., 2003) and dissociative electron attachment (Hanel et al., 2003; Abdoul-Carime et al., 2004). In view of this, an interaction model capable

of giving a realistic, physically meaningful description of the effective genotoxic damage caused by the incident radiation in a biological tissue should improve on existing MC codes in the following aspects:

– The simulation has to take into account the molecular nature of the absorber medium in order to predict the physical or chemical alterations actually induced in its components. On one hand, this means that input data for a given material can no longer be computed as the sum of its atomic constituents, but needs to be supplied specifically for each molecule. On the other hand, it implies that each collision has to be simulated explicitly (event by event), without using approximations treating multiple scattering events as a single process. This approach permits to obtain particle tracks with real nanometric detail.

– All different kinds of known inelastic collisions have to be considered in the interaction model instead of restricting inelastic events exclusively to ionizations. Only by including those inelastic channels, a complete picture of the effects induced in the irradiated medium can be obtained. In particular, all relevant interaction mechanisms leading directly or indirectly to molecular dissociations need to be taken into account. These include, amongst others, neutral dissociation and dissociative electron attachment for causing chemical alterations and radical formation (which, for the particular example of biological materials, can ultimately lead to single or double breaks in RNA or DNA strands and protein malfunctions).

– Finally, low-energy electrons cannot be ignored by the interaction model by applying cut-off values. Electrons should be tracked until thermalization in order to include scattering events that occur only at low energies, even below ionization threshold. By including this amendment, also the circumstance that collectively, low-energy secondary electrons can carry away a considerable amount of energy from the primary particle's path and produce interactions in the surrounding tissue is accounted for. Consequently, interaction data has to be collected for this energy range, as well.

The global aim of a simulation fulfilling these requirements would be to predict radiation damage in biological tissues at the molecular level, ultimately by calculating how exactly specific proteins, DNA strands, or other functional elements are affected by irradiation in particular conditions (nanodosimetric approach). At present, this objective is not resolved due to the still scarce results on radiation-matter interactions for biomolecules. However, here we present the code Low-Energy Particle Track Simulation (LEPTS) which has been specifically designed by us as a tool for nanodosimetry that offers the improvements exposed above. It distinguishes fine details in the electron interaction model and gives a molecular-level description of the processes involved in radiation transport and energy degradation down to about 1 eV. Furthermore, it is a flexible programme prepared to include the results of new investigations as they become available through constant revision and maintenance of the scattering subroutines and the underlying interaction data sets. Apart from electron transport in irradiated materials of biomedical interest, also positron interactions (particularly interesting for imaging applications such as PET, positron emission tomography) can be simulated with LEPTS.

2. Programme structure

The Monte Carlo code used in our simulations (Muñoz et al., 2005; 2007a) is a general purpose code written in C++ that combines our own routines with existing MC programmes. It

LEPTS — a Radiation-Matter InteractionyModel at the
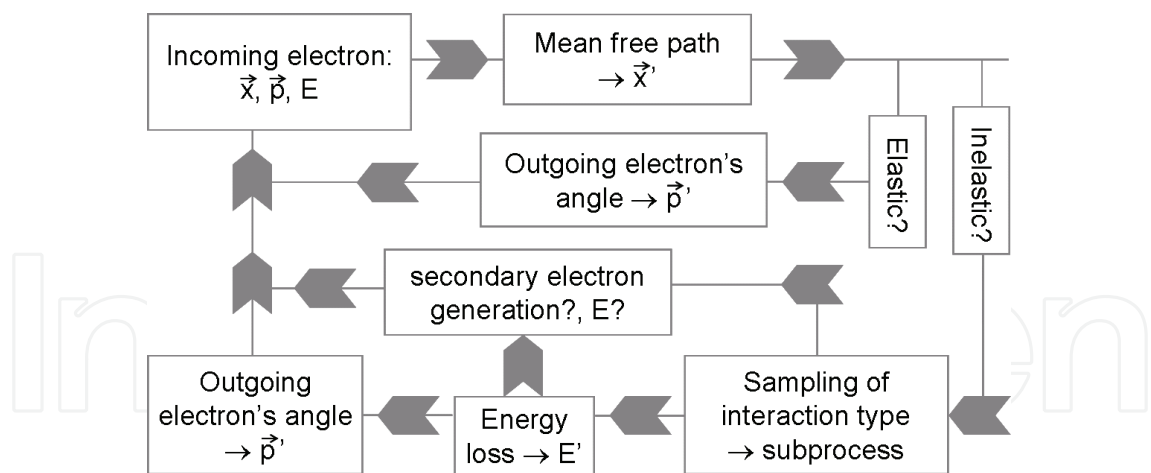Molecular Level and its Use in Biomedical Applications
279

Fig. 1. Diagram depicting how LEPTS handles each collisional event.

uses geometrical and material definition facilities, sampling mechanisms, and graphical output generation from the GEANT4 toolkit (Agostinelli et al., 2003) and is also able to exchange information with PENELOPE (Baró et al., 1995). However, the programme core which provides the functions dealing with the physical interaction processes between incident particles and the target material is LEPTS, the Low-Energy Particle Track Simulation. LEPTS was developed by our group with the main purpose to improve on low-energy and secondary particle interaction models offered by other existing MC codes by providing a molecular-level description of each collisional event until thermalization using experimental input data wherever possible. Currently, electron and positron transport is calculated by LEPTS, while other radiation particles to be tracked in a target material (in particular, photons) are handed over to the corresponding routine available through GEANT-4 or PENELOPE. This combined approach offers the advantages of established radiation transport programmes for tracking many primary particles — whose main effect is to release abundant secondary particles with a certain energy range — in multiple materials on one hand. On the other hand, it provides a complex description of electrons and positrons (whether occurring as primary or secondary particles) including accurate modelling of low-energy processes on a microscopic scale. In recent years, our efforts have centered on adapting LEPTS for use in biomedical applications through the compilation of suitable input parameters and the inclusion of interaction processes that are relevant in biological tissues (e.g., neutral dissociation or electron attachment).

2.1 LEPTS

As has been explained before, the Low-Energy Particle Track Simulation is the central part of our simulation code, the actual interaction model that handles low-energy particles and especially facilitates the simulation of radiation interaction in biological materials (tissues, relevant detector materials, important organic components etc.). It is currently used for processing low-energy electron and positron interactions, typically in the energy range of 1eV up to 1keV. In order to offer a detailed description at the nanoscale, accurate physical models and the selection of input data are equally important. The methods employed in our interaction model for obtaining a realistic simulation at the molecular level are detailed below. A scheme depicting how a radiation-matter interaction event is processed is given in fig. 1. The criteria for input parameter selection will be explained in section 3.

LEPTS is a full Monte Carlo simulation, meaning that each interaction event (collision) is individually simulated starting with the position, direction and energy of the incident particle and giving as an output its new coordinates and energy as well as the possible impact it has caused in the respective molecule of the irradiated material. Unless the incident particle has been absorbed by its interaction partner (for example, via attachment to a molecule in the case of an electron or positronium formation for a positron), the radiation particle after the collision (outgoing particle) is tracked through further scattering events until its thermalization with the surrounding material, at which point it finally deposits the remaining energy. The alterations produced in the absorber, such as local energy deposition, molecular dissociations, or the generation of secondary electrons, are registered by the programme at its exact location within the volume simulated and are available for further analysis at the end of the calculation. Additionally, any secondary particles produced (e.g. through ionization) are always followed by the same means as primary particles until their absorption or thermalization. Given that for most incident radiation qualities, the final energy deposition in the medium is carried out by the multiple secondary electrons produced along the paths of primary particles, this strategy represents a very accurate mode of assessing the radiation damage inflicted.

In order to track an incoming particle, at first, the free path in the medium is sampled according to the total cross section corresponding to its momentary energy. Only once the location of the next collision is thus defined, the interaction model used by LEPTS distinguishes two classes of scattering events: elastic and inelastic scattering. Partial cross sections determine which kind of event is to take place and call the appropriate interaction routine.

For elastic collisions, since no energy is deposited in the medium, the programme samples the outgoing particle's angle according to the distribution established by the corresponding differential cross sections (DCS). In the case of inelastic collisions, different subprocesses (with their relative frequency given by the corresponding partial cross sections) are available depending on the type of incident particle, its energy, and the molecular species encountered. For electron scattering, these processes can currently include ionization (with or without Auger electron generation), vibrational and rotational excitation, electronic excitation, neutral dissociation, and dissociative attachment. In the case of positrons, also positronium formation and annihilation are simulated.

In the next step, the energy lost during the collision is determined. In the case of vibrational or rotational excitations, a fixed value is assigned which only depends on the molecule that was excited and which is calculated as the weighted mean energy of all known levels. For inelastic processes involving complete absorption of the incident particle, the total remaining energy is deposited at the interaction site. For all other inelastic channels, the energy loss is sorted from the energy loss distribution taking into account the threshold applying for a given channel. If different inelastic scattering processes can be clearly distinguished in the underlying energy loss distribution (usually an experimental energy loss spectrum), this is previously split up in order to obtain a specific distribution for each of the respective processes.

Subsequently, the outgoing particle's direction is sampled using the following approximation for the inelastic differential cross section. It has compared well to experimental inelastic DCS for materials like water (Muñoz et al., 2008b) and improves upon other common approximations such as isotropic scattering or using elastic angular distributions directly. For use with LEPTS, the elastic DCS is represented as a function of momentum transfer k to the molecular interaction partner (instead of the outgoing angle θ). Then, the inverse calculation

is done, now taking into account the inelastic nature of the collision being simulated by including an energy loss ΔE.

We thus obtain the outgoing angle after an inelastic scattering event from

$$\cos\theta = \frac{p^2 + p'^2 - k^2}{2\,pp'} \tag{1}$$

where p and p' are incident and final linear momenta, respectively, and the range of k is restricted by $k \in [p - p'; p + p']$.

If an ionization has taken place, a secondary electron is automatically generated and enters the simulation with the energy lost by the primary electron less the ionization energy, moving in the direction obtained when applying linear momentum conservation. Those secondary electrons are then fully tracked in the same way as primary ones until losing all of their energy or exiting the simulated volume. Finally, the interaction event has terminated and the radiation particle is ready to enter the next collision.

Since LEPTS focuses on low-energy interactions, bremsstrahlung photon production is not taken into account by the scattering subroutines currently used in our programme. This circumstance is not expected to introduce observable errors in the applications considered so far due to the relatively low particle energies. The maximum electron energy occurring in the applications presented in section 4 is approximately 3.5 MeV, where the radiation yield amounts to only 1.3 % according to data supplied by the NIST (Berger, 2000).

2.2 Information exchange with other codes

In our combination programme, a simulation is always launched using the GEANT-4 toolkit, meaning that geometrical and material settings are defined there. The initial conditions describing the incident radiation particles are however supplied by the user depending on the situation simulated. In this way, different set-ups can be considered, e.g. parallel incidence / point source / complex source shape, monoenergetic distribution / several discrete energies / continuous incident spectrum, single particle type / mixed incident species, and so on. Once an incident particle with its corresponding coordinates, direction, and energy is thus sampled, other codes can be called for tracking. Electrons and positrons are generally handed over to LEPTS, except for the purpose of comparison between different codes. PENELOPE can be used for simulating photon transport. Other kinds of particles, including photons as well, can be tracked by GEANT-4. Each code is used exclusively with their own, built-in databases.

During particle tracking, individual radiation particles are easily passed over from one programme to another. If, for example, an incident photon undergoes photoelectric effect and thus releases an electron from the absorber material, this is immediately passed over to LEPTS for simulating its further trajectory. No distinction whatsoever is made between primary and secondary particles, all of them being tracked until absorption or thermalization. Therefore, the energy released in a single interaction by any primary radiation particle (in the current example, a photon) when passing through a medium is effectively distributed among the multiple collisions along the paths of the secondary particles generated (electrons) and registered with its exact impact (type of damage induced, energy deposition) on the different absorber molecules that are affected.

Through the assignment of different kinds of particles to a certain code for track simulation, the present combined programme offers a solid base of input data and models plus punctual improvements where needed (for our intended applications, the treatment strictly event by event and the additional detail in the low-energy region). Continuous maintenance and

improvement of LEPTS and its underlying databases ensure that we obtain an up-to-date, versatile simulation model that adapts to multiple needs. Although in principle, the resulting programme is applicable to all kinds of situations, its main advantage is to offer improvements in the simulation of biological materials by accounting for recently discovered mechanisms of radiation damage of great importance at low energies.

3. Input data requirements

It is obvious that an improvement of accuracy and detail in a simulation model has to be accompanied by the corresponding revision and compilation of input parameters in order to be effective. In the present case, particularly low-energy electron and positron interaction data in materials of biomedical interest have to be collected. For each molecular component, this includes total scattering cross sections, integral and angularly differential elastic CS, partial CS for all known inelastic processes, and energy loss distributions (these may include continuous or discrete spectra depending on the collisional process(es) considered).

The interaction database for a given molecular target is compiled by critically revising and joining together published data, often completing them with our own measurements or calculations. Generally, preference is given to experimental results for considering real-life experimental conditions closer to the actual application than the rather idealized initial conditions mostly assumed in theoretical investigations. For best reliability, data are selected from sources that closely agree with other authors, if multiple results have been reported. Theoretical data are referred to when no adequate experimental ones can be encountered or as an additional orientation when different measurements are not conclusive. Mostly, they serve for extrapolating experimental values in order to extend their energy or angular range. Before a set of preferred values is definitely established for partial and total cross sections, a sum check (verifying that for each particle energy, the elastic CS plus the sum of all inelastic channels equals the total CS) is performed in order to test the congruency of the selected data. This "quality assurance" procedure on the final interaction data set helps to reveal error sources such as the inclusion of a single type of collisional event in different inelastic channels (e.g., an electronic excitation and subsequent neutral dissociation of the molecule in principle belongs equally to both partial cross sections) or the failure to discern different interaction channels due to experimental restrictions (as occurs frequently with experimental elastic cross sections that include rotational excitations because of their limited energy resolution).

For many materials, unfortunately the unavailability of sufficient data for all expected collisional processes imposes the main restriction on the accuracy (and thus, also usefulness) of a molecular-level MC simulation. While there are often extensive results on certain processes like elastic scattering or ionization, others like rotational or electronic excitation or even the total scattering cross section tend to exist only for special energy ranges (or certain outgoing angles or excited levels) due to the technical challenge of their measurement or an increased interest only in a particular state. Other channels, such as neutral dissociation, dissociative electron attachment, or positronium formation in the case of positrons, have been barely investigated for many molecules, leading to incomplete data sets that need a considerable amount of extrapolation (which introduces additional uncertainties). This means that while the simulation code can in principle model many kinds of interaction processes (and, at a given point, is easily modifiable in order to incorporate additional ones) at the molecular level, the computational detail attainable is as a matter of fact limited by the availability of suitable and self-consistent input data throughout the desired energy range. As a consequence, in the present state, LEPTS code does not distinguish the exact rotational

or vibrational level after a respective excitation, and does account for the excitation of different electronic states indirectly via the corresponding energy loss distribution. Ionization is always considered to produce a single secondary electron, thus disregarding multiple ionization processes. Also, as inelastic differential CS are only rarely reported (generally, for low energies and even then only for specific conditions), the outgoing particle's angle after inelastic scattering events is approximated as described in section 2.1.

3.1 Data compilation: the example of electrons in H_2O

In the following, data collection and selection is illustrated by the example of electron interactions in water, a relatively well-studied case of electron-molecule scattering. Interaction data compiled here were used for the recent simulations of radiotherapeutic applicators presented in section 4.

3.1.1 Cross section data

The total and partial cross sections needed in order to simulate different electron scattering processes in water were obtained from experimental results whenever possible. Total electron scattering and integral ionization cross sections in water vapour were previously measured in our laboratory between 50 eV and 5 keV (Muñoz et al., 2007b) with a transmission beam technique and using synchronized electron and ion extraction pulses applied to the interaction chamber, respectively. Below 50 eV, total CS data from Čurík et al. (2006) and Szmytkowski (1987) were used. Electron-impact ionization cross sections below 50 eV were taken from Straub et al. (1996). Integral electronic excitation CS have been derived from the electron energy loss analysis carried out by Thorn and co-workers (Thorn et al., 2007a; Brunger et al., 2008; Thorn et al., 2007b) from 15 to 50 eV and have been extrapolated down to threshold and up to higher energies by assuming a double logarithmic dependence with energy. Vibrational excitation and electron attachment cross sections were taken from the recommendations made by Itikawa & Mason (2005).

For elastic collisions and neutral dissociation, integral cross sections were determined by combining experimental data and our own theoretical calculations. These were carried out with an optical potential method based on an independent atom approximation including screening corrections. Further details regarding the calculations can be found in Blanco & García (2003a;b; 2007). The model approach considers inelastic scattering as electron-electron interactions, consequently both vibrational excitation and electron attachment are excluded. Thus, when subtracting the ionization and the electronic excitation cross sections from the calculated integral inelastic cross sections, the resulting data should correspond to neutral dissociation. The good agreement with experimental results (Kedzierski et al., 1998; Harb et al., 2001) confirms this assignment. Elastic cross sections are based on experimental data from Cho et al. (2004) but include a correction for contamination with rotationally inelastic scattering. The CS values for rotational excitation are included in simulations only when considering water in the gas phase. Further details can be found in Muñoz et al. (2008b).

For high energies, the electron-molecule collision can be treated as a plane wave interaction with a sum of atoms in the framework of the first Born approximation. Integral elastic and inelastic interaction cross sections can then be represented by simple energy-dependent formulae (García & Blanco, 2000; Inokuti, 1971). For want of other data, this method was used at energies $\geq$ 10 keV. Angular distribution functions for scattered electrons were taken from our calculations, using the approximation described in section 2.1 for inelastic collisions.
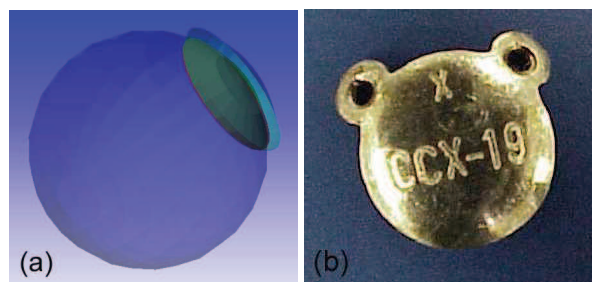
Fig. 2. Ru/Rh applicator used for the present simulation: (a) Scheme of the plaque placed around the eyeball. (b) Photo of the CCX plaque (Bebig, Germany).

3.1.2 Electron energy loss distributions

Electron energy loss distributions in H_2O were measured by us in a transmission beam set-up in order to assign the energy released in each electron-molecule interaction. After observing that the energy loss distributions did not present significant variations (uncertainty $\leq 15\%$) for incident electron energies in the range 50–5 000 eV, a unique (average) electron energy loss spectrum was used (Muñoz et al., 2008a). The mean excitation energy in water yielded by this distribution is ≤ 34 eV for electron energies ≤ 500eV and rises to about 40 eV for energies beyond the threshold for inner shell excitation/ionization.

4. Recent applications to radiotherapy

Radiotherapy of many tumours requires increased spatial precision due to the sometimes small dimensions of the treatment volume and the close proximity of organs at risk. A high accuracy energy deposition model might thus improve dose calculations (and, consequently, treatment planning and outcome). Motivated by this, the MC simulation LEPTS has been applied to determine the energy deposition in water of two radionuclides commonly used in brachytherapy, ruthenium-106 and iodine-125. The electron transport model capable of providing detailed information about secondary electron tracks, energy deposition and interaction processes at the molecular level can yield a completer picture of radiation damage in a biomedical context. In both cases, the radiation spectra emitted by the therapeutic applicators were measured by us in order to provide realistic input data and to reproduce incident radiation spectra accurately in the simulation. The localized dose deposition by both radionuclides benefits treatment outcome by sparing healthy patient tissues while delivering high doses to the clinical target volume. At the same time, these isotopes are suitable for longer-term or permanent implants, assuring the radioprotection of medical staff and third persons in close contact with patients.

The present simulations use data corresponding to a molecular medium in the gas phase without correcting for any collective effects present in liquid water. However, based on the very similar electron mass stopping powers obtained for water vapour and liquid H_2O in the keV range (Muñoz et al., 2007b), no major differences are expected when considering the liquid phase.

4.1 Ocular brachytherapy with [106]Ru

First, LEPTS is used to simulate brachytherapy of the eye with the beta-emitter [106]Ru. Uveal melanoma and other malignancies of the eye can be effectively treated by surgically implanting a concave ruthenium applicator tightly around the eyeball. As the ocular medium
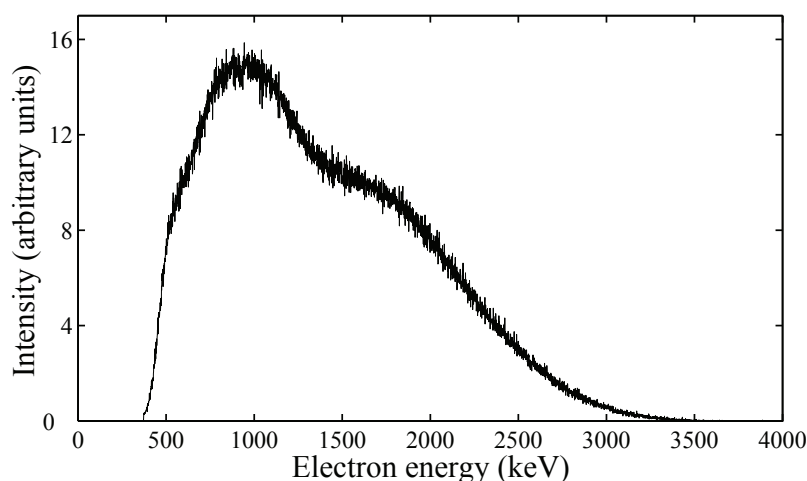
Fig. 3. Beta emission spectrum of the CCX type ophthalmic Ru-106 plaque.

can easily be mimicked by water, it constitutes an excellent system for applying the present simulation model with the interaction data set presented in section 3.1.

[106]Ru is a β-emitter (endpoint energy 39.4 keV) that slowly ($T_{1/2}$ = 373.59 d) decays to [106]Rh with which it reaches secular equilibrium: it has a half-life period of 29.8 s before decaying to [106]Pd (stable) by different beta decays with a maximum energy of 3.541 MeV. Subsequent γ emissions from palladium have a maximum energy of 1.5623 MeV. Other probable decay energies are 2.407 MeV, 3.029 MeV and 1.979 MeV (β) and 511.86 keV, 621.93 keV and 1.050 MeV (γ) (data from the Lund Nuclear Data Service: Chu et al. (1999)). The combined electron emission spectrum of the applicator for use in the simulation was determined experimentally (Muñoz et al., 2008a) with a silicon detector and is shown in fig. 3. Note that the lowest-energy electrons emitted directly from ruthenium are absorbed within the applicator material, reducing the applicator's effective emission to the keV–MeV spectrum of its daughter nucleus rhodium.

Photon emission spectra that were measured with standard solid state spectrometers (Muñoz et al., 2008a) in order to check for a possible contamination of the source revealed gamma energies in excellent agreement with the disintegration scheme. However, in order to quantitatively relate electron and photon radiation, relative intensities of the γ emissions were taken from Chu et al. (1999).

Using a generic setup frequently found in brachytherapy of the eye with concave Ru/Rh plaques (c.f. figure 2), radiation-induced processes in the volume of interest - the eyeball approximated by liquid water - have been simulated. For this application, the incident photons were simulated using the photon interaction processes integrated in GEANT4. Once a secondary electron is generated, it is tracked using LEPTS. As the programme output, we thus obtain the exact location of each interaction event as well as the type of collision produced, the energy deposited, the change of momentum suffered by the particle, and the energy and direction of the secondary electron produced in case of ionizations.

Figure 4 shows lateral and transversal sections through the energy deposition map calculated after simulating approximately 2×10^6 primary particle histories (not taking into account those tracks that leave the volume of interest in the opposite direction, without entering the eye). (The applicator — not shown — is located to the left of the eyeball.) As expected for an efficient treatment of uveal melanoma and other tumours that are located similarly, bordering the vitreous humour, one obtains a steep dose gradient close to the applicator that becomes
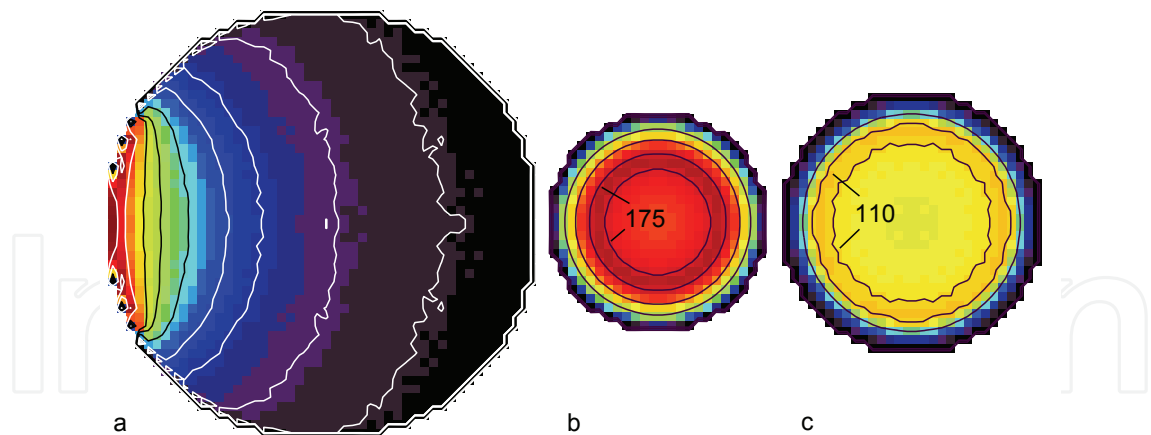
Fig. 4. Relative dose distributions produced by the ^{106}Ru plaque in the eyeball simulated as water (voxel size: $0.5 \times 0.5 \times 0.5$ mm^2). (a) Longitudinal section through the central axis of the applicator with 200%, 150%, 100%, 75%, 50%, 30%, 20%, 10% and 5% isodose lines shown. (b) Transversal section in 1 mm depth displaying 175%, 125% and 75% lines. (c) Transversal section in 2 mm depth displaying 110% and 50% lines. The same colourmap is used for all distributions.

flatter towards the centre of the eye. After normalization of dose to 100% in 2 mm depth, the relative dose absorbed in the first voxel (0-0.5mm depth) amounts to 249%, then decays to 55% in 4 mm depth (all at central axis). The relative depth dose curve along the central axis, applying the same normalization, is shown in figure 5. It can be seen that on one hand, the dose gradient is very steep within the first few mm inside the eye, but on the other hand there is still a considerable amount of energy deposited in greater depths (approximately 16% in 1 cm depth and 4% in 2 cm depth). This is due to the applicator geometry with a curved surface, the greater penetration of incident photons (compared to electrons which account for the main dose in the entrance region), and secondary electrons depositing small amounts of energy in multiple collisions while slowing down continuously. Lateral dose profiles for many different
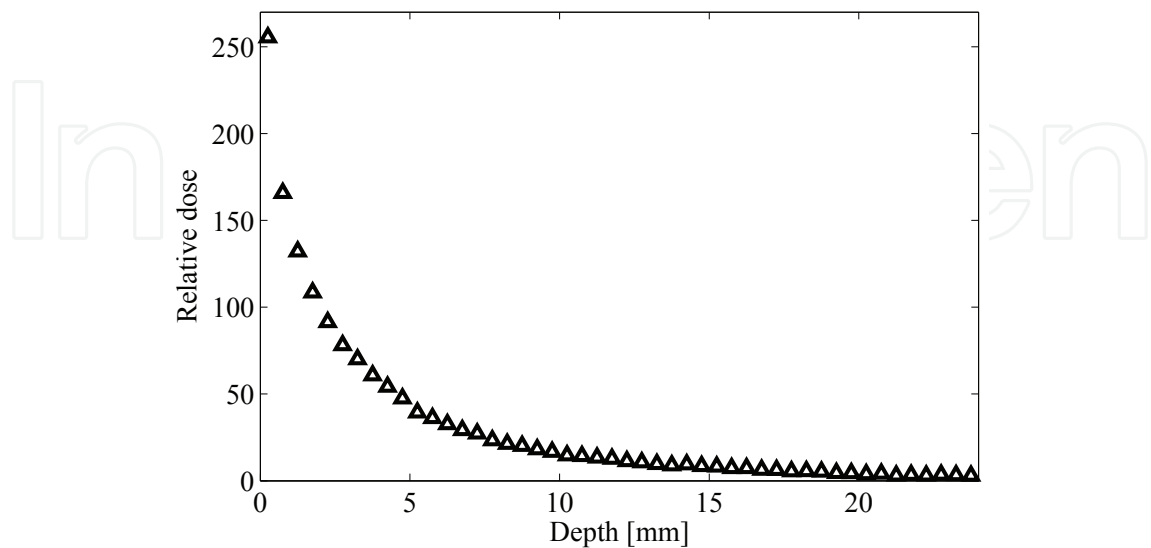

Fig. 5. Relative depth dose deposited at the central axis of the water eyeball by a CCX type Ru/Rh applicator. Normalization as in figure 4
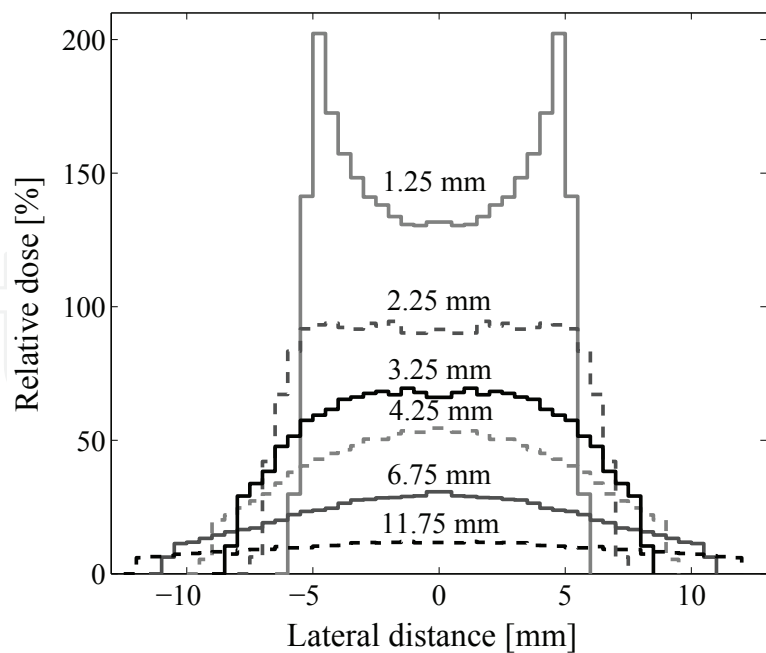
Fig. 6. Lateral dose profiles obtained for different depths in the eyeball (water sphere). Data is normalized to 100% in 2 mm depth.

depths are presented in figure 6. They exhibit two pronounced maxima in the region close to the applicator (up to 2 mm depth), reflecting its concave shape, an essentially flat central part in 2.25 mm depth, and a single, broader maximum in greater depths.

In this application, an ophthalmic brachytherapy plaque placed around the eye has been simulated by employing LEPTS for electron tracking and making use of the geometry definition facilities offered by GEANT-4, as well as its photon interaction routines. When comparing the dose distribution calculated with previous results obtained with PENELOPE on similar applicators (Sánchez-Reyes et al., 1998), they seem to be consistent within the first millimeters inside the eyeball. In depths $\geq$ 4 mm, the present simulation shows a shallower slope and yields larger doses at the central axis. Two possible causes are the additional dose delivered by the γ component — not accounted for in the other study — which steadily gains importance for greater depths within the medium and differences in the β spectrum used (theoretical vs. experimental spectrum). Finally, the differences in the scattering model and/or the underlying interaction data set might be responsible for the discrepancies encountered. A comparison of results obtained with PENELOPE and LEPTS in identical conditions (plaque and eye geometry, incident spectra) would be needed in order to confirm or discard the last possibility.

4.2 Brachytherapy with ^{125}I seeds

Here we show en example of how LEPTS is combined with PENELOPE in order to simulate the interaction of photon radiation with water. In particular, we investigate photon radiation with an initial energy distribution as measured for ^{125}I seeds that are used for radiotherapy of prostate cancers but can also be employed for treating lesions affecting the eye. Therefore, we do not assume any specific geometry here but center on an accurate representation of the emitted radiation and its penetration in water.

For obtaining the incident radiation spectrum in this application, a solid state Si(Li) spectrometer was used to determine the energy and intensity of the photons emitted by a
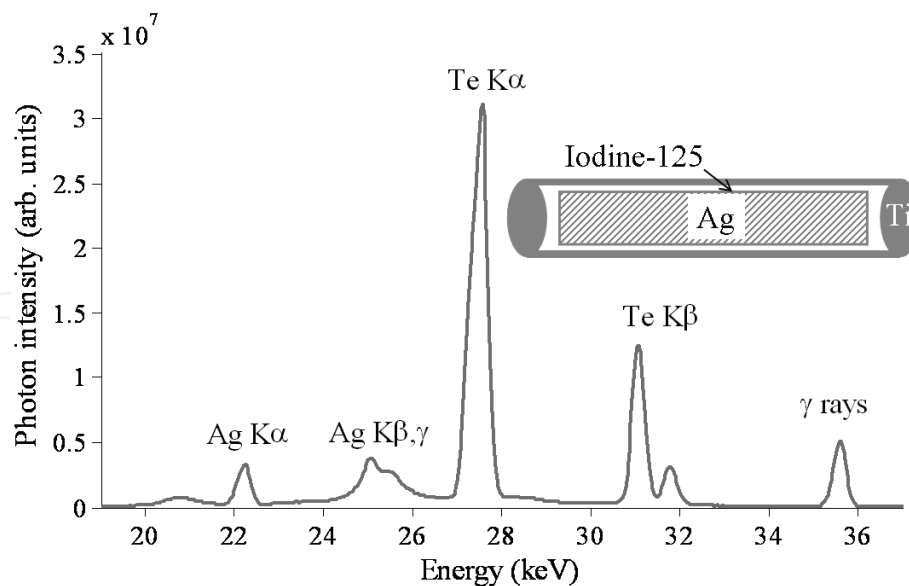
Fig. 7. Photon emission spectrum of the Amersham Health model 6711 ^{125}I seed as measured in perpendicular geometry. Gamma photons (35.49 keV) produced during ^{125}I/[125]Te-decay as well as the most intense Kα and Kβ X-rays of Te are observed.

[125]I brachytherapy seed (see fig. 7). [125]I decays to the 35.49 keV state of [125]Te by electron capture (half-life: 59.408 days) with 100% probability. The subsequent relaxation of nucleus and shell causes a gamma and X-ray photon emission which is considered as the primary radiation in this model. A representative spectrum shows the γ peak and various X-ray lines of tellurium in the range 27-32 keV. Additionally, X-ray lines between 22 and 26 keV with an intensity comparable to some of the photons emitted by Te were observed which are attributed to silver (present as the core of the seed onto which the radioactive iodine is adsorbed). These "contaminations" of the spectrum need to be taken into account for realistically modelling applications in brachytherapy (Rivard et al., 2004), and are thus included.

Using LEPTS in combination with PENELOPE (as explained in section 2.2), we simulated the interaction processes induced in water vapour when exposed to photon radiation according to the emission spectrum presented above. The resulting interaction map with H_2O molecules, at a density similar to that of liquid water, is shown in fig. 8. Note that up to this point, where exclusively interactions caused directly by photons are considered, only PENELOPE is used. It can be observed that in the geometry used, the photon beam remains laterally well defined, however some photon interaction events can be found even near the boundary of the simulated volume and release secondary electrons there. Photon interactions are coloured according to the type of event produced. Note that photoeffect (red dots) prevails for I-125 in water (which, for many purposes, is an acceptable approximation for human tissue), indicating that the main effect of the incident photons is to generate high-energy secondary electrons. These new electrons subsequently continue the energy deposition process by undergoing multiple scattering events until their thermalization. In this "second generation" of energy deposition events, PENELOPE is no longer involved, but electron-molecule collisions are individually simulated by LEPTS. In figure 9, one photoelectron track shown from its generation until complete thermalization, illustrates details of the energy degradation mechanism. It can be seen which different inelastic interactions with target molecules the secondary particle undergoes and how it deposits energy at many points along its track. Furthermore, additional electrons are generated by ionization events. This highlights the
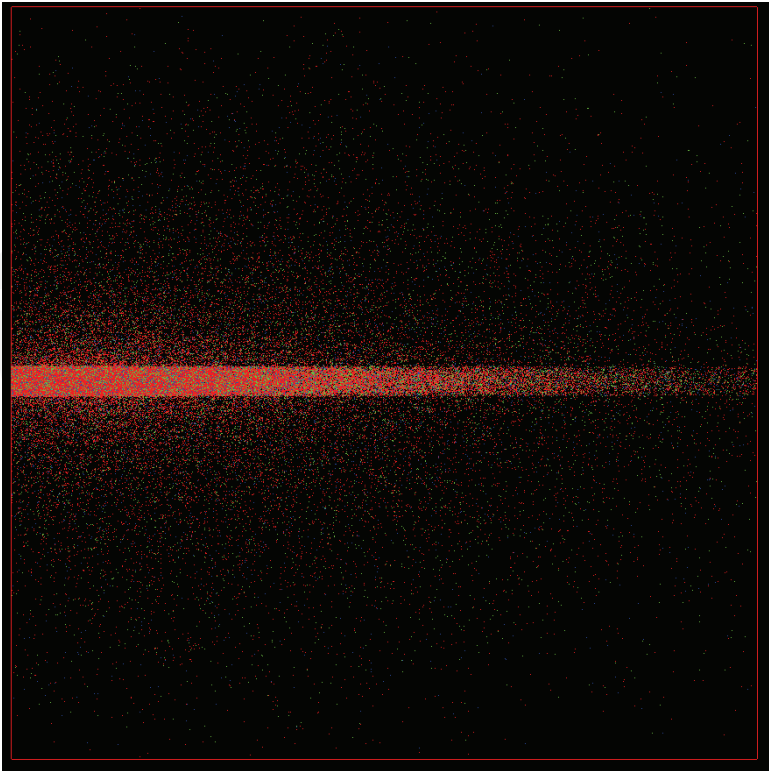
Fig. 8. Simulation of 100 000 photons emitted from a 4 mm (diameter) disk according to the energy distribution measured for I-125 seeds used in brachytherapy. The simulated volume (red box) consists of $10\times10\times10$ cm^3 of water vapour at a density of 0.7320 g/cm^3. Different types of interactions are colour-coded as follows: red, photoelectric effect; green, Compton scattering; blue, Rayleigh scattering.

necessity to include accurate electron interaction data and models into simulation approaches for medical applications, as is done in the present Monte Carlo model, even if the primary radiation consists of photons as with I-125.
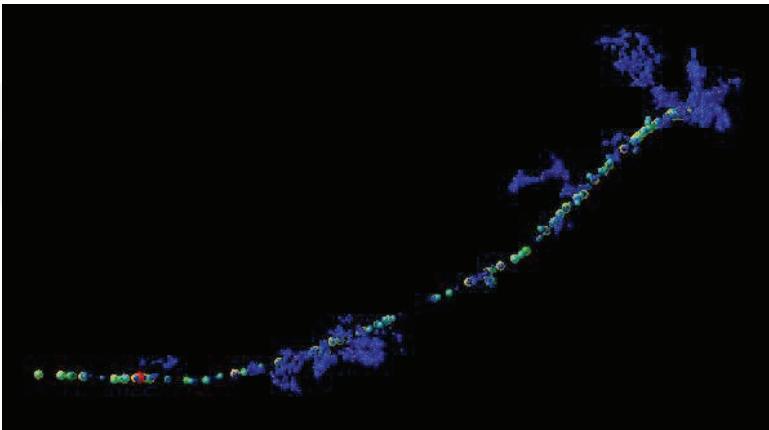

Fig. 9. Example of a photoelectron trajectory (from lower left to upper right) showing details about the electron-molecule interactions produced. Collisions are depicted using orange (ionization), yellow (neutral dissociation), green (electronic excitation), cyan (vibrational excitation), light blue (rotational excitation), and dark blue (elastic collision). For clarity, only some of the numerous elastic collisions are shown.
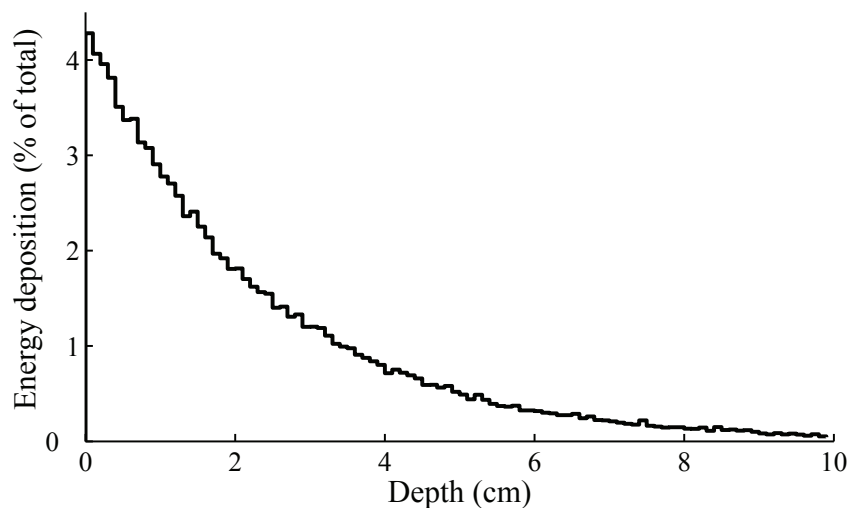
Fig. 10. Histogram showing the energy deposition by an I-125 source in water vapour at a density of 0.7320 g/cm^3 and supposing parallel photon emission. All contributions for a given depth are summed. The total energy deposited in the simulated volume ($10\times10\times10$ cm^3) is normalized to 100%.

Figure 10 depicts the energy deposition (equivalent to the relative depth dose curve) corresponding to a parallel photon beam of 4 mm diameter penetrating water at a density of 0.7320 g/cm^3. Most of the incident energy is lost immediately after entrance into the medium. 58.4% of the total energy is deposited within the first 2 cm, and 90% of the energy is deposited within 5.1 cm.

I-125 is used for radiotherapy of different tumours including ocular tumours which require a high spatial precision due to the small dimensions of the treatment volume and the close proximity of organs at risk such as the optical nerve, eye lens, lachrymal gland, etc. Simulation with a detailed energy deposition model, including an accurate representation of secondary electron interactions, thus improves dose calculations and may help to spare healthy tissues while effectively irradiating the target volume. In order to validate the present approach using LEPTS/PENELOPE for applications to radiotherapy with photon radiation, further studies will be aimed at a more realistic simulation of typical clinical cases (prostate/eye cancers), including exact geometries of radiation sources and of the relevant patient tissues.

5. Conclusions and outlook

We have presented a MC simulation code that introduces improvements in low-energy particle tracking compared to some other, currently widely used programmes (Kawrakow, 2000; Brown, 2003; Baró et al., 1995; Agostinelli, 2003). It offers a molecular-level description of the different interactions taking place between radiation particles and the traversed medium as well as a tracking model that follows electrons and positrons until thermalization. By not using any condensed-history algorithms, a series of problems that have been reported for other codes (Poon & Verhaegen, 2005; Poon et al., 2005; Bousis et al., 2008) are naturally excluded. Obviously, however, this also considerably increases the calculational resources (processing time) needed. Input data are carefully selected for each molecular material to be simulated and are updated as needed. As a result, the present simulation programme constitutes a useful tool for incorporating our knowledge on the molecular mechanisms of radiation damage into macroscopic applications and thus facilitating nanodosimetry.

Whilst the present simulation LEPTS cannot compete with the computational speed achieved by the state-of-the-art MC codes currently used for dose calculations in biomedical applications (particularly, in radiation therapy), its special treatment of low-energy particles and detailed modelling of inelastic scattering events yields a different view on radiation damage at the nanoscale by taking into account the molecular nature of the absorber medium. It could therefore give valuable clues by comparing LEPTS results with the ones obtained by other codes when considering typical "standard" situations in radiotherapy, radioprotection or medical imaging techniques (e.g., positron emission tomography). Also, a comparison of the predicted molecular-level damage due to irradiation in a tissue with the effect caused by the same irradiation at organic level will be of great interest.

Two examples of application to radiotherapy have been studied, both based on electron interaction data with water (which represents a good approximation for biological tissues for many purposes). Other data sets for use with LEPTS existing at the moment include those describing electron interactions in air (Muñoz et al., 2005), methane (CH_4, Fuss et al. (2010)) and ethylene (C_2H_4) (these two for representing simple hydrocarbons, basic building blocks in biology) and positron interactions in argon and water. A database on electron scattering by tetrahydrofuran (THF, C_4H_8O), a molecule interesting due to its strong similarity with the pentose forming part of nucleotides, is currently in preparation. With these data at our disposal, positron tracking during PET diagnostics and the simulation of electrons in THF are the next applications planned for the near future. Furthermore, particle tracking in materials composed of various different molecules will be carried out.

6. References

Abdoul-Carime, H., Gohlke, S. & Illenberger, E. (2004). Site-specific dissociation of DNA bases by slow electrons at early stages of irradiation, *Phys. Rev. Lett.* 92: 168103.

Agostinelli, S. et al. (2003). GEANT4 – a simulation toolkit, *Nucl. Instrum. Meth. A* 506: 250–303.

Badano, A. & Sempau, J. (2006). MANTIS: combined x-ray, electron and optical Monte Carlo simulations of indirect radiation imaging systems, *Phys. Med. Biol.* 51: 1545–1561.

Baró, J., Sempau, J., Fernández-Varea, J. M. & Salvat, F. (1995). PENELOPE: An algorithm for Monte Carlo simulation of the penetration and energy loss of electrons and positrons in matter, *Nucl. Instrum. Meth. B* 100: 31–46.

Berger M. J. (National Institute of Standards and Technology) (2000). Stopping-power and range tables for electrons. Available from: http://physics.nist.gov/PhysRefData/Star/Text/ESTAR.html.

Berger, M. & Seltzer, S. (1973). *ETRAN Monte Carlo code system for electron and photon transport through extended media, Radiation Shielding Information Center (RSIC) Report CCC-107*, Oak Ridge National Laboratory, (Oak Ridge, TN).

Blanco, F. & García, G. (2003a). Improvements on the quasifree absorption model for electron scattering, *Phys. Rev. A* 67: 022701.

Blanco, F. & García, G. (2003b). Screening corrections for calculation of electron scattering from polyatomic molecules, *Phys. Lett. A* 317: 458–462.

Blanco, F. & García, G. (2007). Calculated cross sections for electron elastic and inelastic scattering from DNA and RNA bases, *Phys. Lett. A* 360: 707.

Boudaïffa, B., Cloutier, P., Hunting, D., Huels, M. A. & Sanche, L. (2000). Resonant formation of DNA strand breaks by low-energy (3 to 20 eV) electrons, *Science* 287: 1658–1660.

Bousis, C., Emfietzoglou, D., Hadjidoukas, P. & Nikjoo, H. (2008). A Monte Carlo study of absorbed dose distributions in both the vapor and liquid phases of water

by intermediate energy electrons based on different condensed-history transport schemes, *Phys. Med. Biol.* 53: 3739–3761.

Brown, F. B. (2003). *MCNP–A general Monte Carlo-particle transport code, version 5*, *Technical Report LA-UR-03*, Los Alamos National Laboratory, (Los Alamos, NM).

Brunger, M. J., Thorn, P. A., Campbell, L., Diakomichalis, N., Kato, H., Kawahara, H., Hoshino, M., Tanaka, H. & Kim, Y.-K. (2008). Excitation of the lowest lying $^3B_1$, $^1B_1$, $^3A_2$, $^1A_2$, $^3A_1$ and $^1A_1$ electronic states in water by 15 eV electrons, *Int. J. Mass Spectrom.* 271: 80–84.

Cho, H., Park, Y. S., Tanaka, H. & Buckman, S. J. (2004). Measurements of elastic electron scattering by water vapour extended to backward angles, *J. Phys. B* 37: 625–634.

Chu, S., Ekström, L. & Firestone, R. (1999). The Lund/LBNL nuclear data search, http://nucleardata.nuclear.lu.se/ nucleardata/toi/.

Cullen, D., Hubbell, J. H. & Kissel, L. (1997). *The Evaluated Photon Data Library, '97 Version*, *Technical Report UCRL-LR-50400 vol 6*, Lawrence Livermore National Laboratory, (Livermore, CA). rev 5.

Čurík, R., Ziesel, J. P., Jones, N. C., Field, T. A. & Field, D. (2006). Rotational excitation of H_2O by cold electrons, *Phys. Rev. Lett.* 97: 123202.

Fuss, M., Muñoz, A., Oller, J., Blanco, F., Hubin-Franskin, M.-J., Almeida, D., Limão-Vieira, P. & García, G. (2010). Electron-methane interaction model for the energy range 0.1-10000 eV, *Chem. Phys. Lett.* 486: 110–115.

García, G. & Blanco, F. (2000). Energy dependence of the total cross section for electron scattering by chloromethanes in the energy range 0.5-10 keV, *Phys. Rev. A* 62: 044702.

Halbleib, J. A. & Melhorn, T. A. (1984). *ITS: The integrated TIGER series of coupled electron/photon Monte Carlo transport codes*, *Sandia Report SAND840573*, Sandia National Laboratory, (Albuquerque, NM).

Hanel, G., Gstir, B., Denifl, S., Scheier, P., Probst, M., Farizon, B., Farizon, M., Illenberger, E. & Märk, T. D. (2003). Electron attachment to uracil: Effective destruction at subexcitation energies, *Phys. Rev. Lett.* 90: 188104.

Harb, T., Kedzierski, W. & McConkey, J. W. (2001). Production of ground state OH following electron impact on H_2O, *J. Chem. Phys.* 115: 5507–5512.

Hubbell, J. H., Berger, M. J. & Seltzer, S. M. (1985). X-ray and gamma ray cross sections and attenuation coefficients, *Standard Reference Database 8*, National Institute of Standards and Technology.

Hubbell, J. H., Veigele, W. J., Briggs, E. A., Brown, R. T., Cromer, D. T. & Howerton, R. J. (1975). Atomic form factors, incoherent scattering functions and photon scattering cross sections, *J. Phys. Chem. Ref. Data* 4: 471–538.

Huels, M. A., Boudaïffa, B., Cloutier, P., Hunting, D. & Sanche, L. (2003). Single, double, and multiple double strand breaks induced in DNA by 3–100 eV electrons, *J. Am. Chem. Soc.* 125: 4467–4477.

ICRU (1984). Stopping powers for electrons and positrons, *Technical Report 37*, International Commission on Radiation Units and Measurements.

Inokuti, M. (1971). Inelastic collisions of fast charged particles with atoms and molecules—the Bethe theory revisited, *Rev. Mod. Phys.* 43: 297–347.

Itikawa, Y. & Mason, N. (2005). Cross sections for electron collisions with water molecules, *J. Phys. Chem. Ref. Data* 34: 1–22.

Jan, S. et al. (2004). GATE: a simulation toolkit for PET and SPECT, *Phys. Med. Biol.* 49: 4543–4561.

Kawrakow, I. (2000). Accurate condensed history Monte Carlo simulation of electron transport: I. EGSnrc, the new EGS4 version, *Med. Phys.* 27: 485–498.

Kedzierski, W., Derbyshire, J., Malone, C. & McConkey, J. W. (1998). Isotope effects in the electron impact break-up of water, *J. Phys. B* 31: 5361–5368.

Muñoz, A., Blanco, F., García, G., Thorn, P. A., Brunger, M. J., Sullivan, J. P. & Buckman, S. J. (2008b). Single electron tracks in water vapour for energies below 100 eV, *Int. J. Mass Spectrom.* 277: 175–179.

Muñoz, A., Blanco, F., Oller, J. C., Pérez, J. M. & García, G. (2007a). Energy deposition models at the molecular level in biological systems, *Adv. Quant. Chem.* 52: 21–57.

Muñoz, A., Oller, J. C., Blanco, F., Gorfinkiel, J. D., Limão-Vieira, P. & García, G. (2007b). Electron-scattering cross sections and stopping powers in H_2O, *Phys. Rev. A* 76: 052707.

Muñoz, A., Oller, J. C., Blanco, F., Gorfinkiel, J. D., Limão-Vieira, P., Maira-Vidal, A., Borge, M. J. G., Tengblad, O., Huerga, C., Téllez, M. & García, G. (2008a). Energy deposition model based on electron scattering cross section data from water molecules, *J. Phys. Conf. Ser.* 133: 012002.

Muñoz, A., Pérez, J. M., García, G. & Blanco, F. (2005). An approach to Monte Carlo simulation of low-energy electron and photon interactions in air, *Nucl. Instrum. Meth. A* 536: 176–188.

Perkins, S. T., Cullen, D. E., Chen, M. H., Hubbell, J. H., Rathkopf, J. & Scofield, J. (1991b). Tables and graphs of atomic subshell and relaxation data, derived from the LLNL Evaluated Atomic Data Library (EADL), Z=1100, *UCRL-50400 30*, LLNL.

Perkins, S. T., Cullen, D. E. & Seltzer, S. M. (1991a). Tables and graphs of electron-interaction cross sections from 10 ev to 100 GeV, derived from the LLNL Evaluated Electron Data Library (EEDL), *UCRL-50400 31*, LLNL.

Poon, E., Seuntjens, J. & Verhaegen, F. (2005). Consistency test of the electron transport algorithm in the GEANT4 Monte Carlo code, *Phys. Med. Biol.* 50: 681–694.

Poon, E. & Verhaegen, F. (2005). Accuracy of the photon and electron physics in GEANT4 for radiotherapy applications, *Med. Phys.* 32: 1696–1711.

Reynaert, N., van der Marck, S. C., Schaart, D. R., Van der Zee, W., Van Vliet-Vroegindeweij, C., Tomsej, M., Jansen, J., Heijmen, B., Coghe, M. & De Wagter, C. (2007). Monte Carlo treatment planning for photon and electron beams, *Rad. Phys. Chem.* 76: 643–686.

Rivard, M J and, C. B. M., DeWerd, L. A., Hanson, W. F., Huq, M. S., Ibbott, G. S., Mitch, M. G., Nath, R. & Williamson, J. F. (2004). Update of AAPM Task Group No. 43 Report: A revised AAPM protocol for brachytherapy dose calculations, *Med. Phys.* 31: 633.

Sánchez-Reyes, A., Tello, J. J., Guix, B. & Salvat, F. (1998). Monte Carlo calculation of the dose distributions of two [106]Ru eye applicators, *Radiother. Oncol.* 49: 191–196.

Seltzer, S. M. & Berger, M. J. (1985). Bremsstrahlung spectra from electron interactions with screened atomic nuclei and orbital electrons, *Nucl. Instrum. Meth. B* 12: 95.

Storm, E. & Israel, H. I. (1970). Photon cross sections from 1 keV to 100 MeV for elements Z=1 to Z=100, *At. Nucl. Data Tables* 7: 565–681.

Straub, H. C., Renault, P., Lindsay, B. G., Smith, K. A. & Stebbings, R. F. (1996). Absolute partial cross sections for electron-impact ionization of H_2, N_2, and O_2 from threshold to 1000 eV, *Phys. Rev. A* 54: 2146–2153.

Szmytkowski, C. (1987). Absolute total cross sections for electron-water vapour scattering, *Chem. Phys. Lett.* 163: 363–367.

Thorn, P. A., Brunger, M. J., Kato, H., Hoshino, M. & Tanaka, H. (2007b). Cross sections for the

electron impact excitation of the $\tilde{a}^3 b_1$, $\tilde{b}^3 a_1$ and $\tilde{B}^1 A_1$ dissociative electronic states of water, *J. Phys. B* 40: 697–708.

Thorn, P. A., Brunger, M. J., Teubner, P. J. O., Diakomichalis, N., Maddern, T., Bolorizadeh, M. A., Newell, W. R., Kato, H., Hoshino, M., Tanaka, H., Cho, H. & Kim, Y.-K. (2007a). Cross sections and oscillator strengths for electron-impact excitation of the $\tilde{A}^1 B_1$ electronic state of water, *J. Chem. Phys.* 126: 064306.

Verhaegen, F. & Seuntjens, J. (2003). Monte Carlo modelling of external radiotherapy photon beams, *Phys. Med. Biol.* 48: R107–R164.
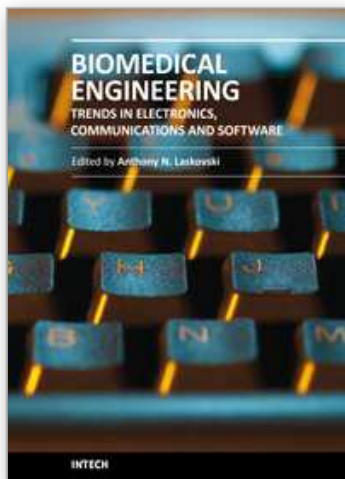
Biomedical Engineering, Trends in Electronics, Communications and Software

Edited by Mr Anthony Laskovski

ISBN 978-953-307-475-7

Hard cover, 736 pages

Publisher InTech

Published online 08, January, 2011

Published in print edition January, 2011

Rapid technological developments in the last century have brought the field of biomedical engineering into a totally new realm. Breakthroughs in materials science, imaging, electronics and, more recently, the information age have improved our understanding of the human body. As a result, the field of biomedical engineering is thriving, with innovations that aim to improve the quality and reduce the cost of medical care. This book is the first in a series of three that will present recent trends in biomedical engineering, with a particular focus on applications in electronics and communications. More specifically: wireless monitoring, sensors, medical imaging and the management of medical information are covered, among other subjects.

How to reference

In order to correctly reference this scholarly work, feel free to copy and paste the following:

Martina Fuss, Ana G. Sanz, Antonio Muñoz, Francisco Blanco, Marina Téllez, Carlos Huerga and Gustavo Garcia (2011). LEPTS – a Radiation-Matter Interaction Model at the Molecular Level and its Use in Biomedical Applications, Biomedical Engineering, Trends in Electronics, Communications and Software, Mr Anthony Laskovski (Ed.), ISBN: 978-953-307-475-7, InTech, Available from:

http://www.intechopen.com/books/biomedical-engineering-trends-in-electronics-communications-and-software/lepts-a-radiation-matter-interaction-model-at-the-molecular-level-and-its-use-in-biomedical-applicat

INTECH
open science | open minds